Experimental and Theoretical Studies on the Magnetic Anisotropy in Lanthanide(III)-Centered Fe_3Ln Propellers**

Luca Rigamonti,[a] Andrea Nava,[a, b] Marie-Emmanuelle Boulon,[c, d] Javier Luzon,[e, f] Roberta Sessoli,*[c] and Andrea Cornia*[a]

Abstract: Compounds $[Fe_3Ln(tea)_2(dpm)_6]$ (**Fe_3Ln**; Ln = Tb–Yb, H_3tea = triethanolamine, Hdpm = dipivaloylmethane) were synthesized as lanthanide(III)-centered variants of tetrairon(III) single-molecule magnets (Fe_4) and isolated in crystalline form. Compounds with Ln = Tb–Tm are isomorphous and show crystallographic threefold symmetry. The coordination environment of the rare earth, given by two tea^{3-} ligands, can be described as a bicapped distorted trigonal prism with D_3 symmetry. Magnetic measurements showed the presence of weak ferromagnetic Fe···Ln interactions for derivatives with Tb, Dy, Ho, and Er, and of weak antiferromagnetic or negligible coupling in complexes with Tm and Yb. Alternating current susceptibility measurements showed simple paramagnetic behavior down to 1.8 K and for frequencies reaching 10000 Hz, despite the easy-axis magnetic anisotropy found in **Fe_3Dy**, **Fe_3Er**, and **Fe_3Tm** by single-crystal angle-resolved magnetometry. Relativistic quantum chemistry calculations were performed on **Fe_3Ln** (Ln = Tb–Tm): the ground J multiplet of Ln^{3+} ion is split by the crystal field to give a ground singlet state for Tb and Tm, and a doublet for Dy, Ho, and Er with a large admixture of m_J states. Gyromagnetic factors result in no predominance of g_z component along the threefold axis, with comparable g_x and g_y values in all compounds. It follows that the environment provided by the tea^{3-} ligands, though uniaxial, is unsuitable to promote slow magnetic relaxation in **Fe_3Ln** species.

Introduction

Single-molecule magnets (SMMs) are molecular compounds that can be in principle used to store and process information because of their magnetic bistability and quantum behavior.[1,2] In essence, a SMM is a magnetic molecule whose magnetic moment aligns preferentially along a specific molecular axis ("easy-axis" anisotropy) and switches very slowly between the two equivalent directions. Since such properties require low temperatures to be observed (< 4.2 K in most cases), an important target of research is the design of new systems that outperform known SMMs[3–6] in terms of operating temperature. Compounds containing 4f ions are very promising in this respect,[4–6] since crystal field (CF) effects in lanthanides are weak and orbital momentum remains largely unquenched, resulting in huge magnetic anisotropies. In mononuclear lanthanide(III) complexes the sign of anisotropy ("easy-axis" or "easy plane") and the possibility to observe SMM behavior have been related by Long et al. to the spatial distribution of the 4f-electron cloud and of ligand charges.[7] More recently, Chilton et al. expanded this approach from a theoretical point of view proposing an electrostatic model in which the magnetic anisotropy of dysprosium(III) complexes can be calculated by considering the charges of the coordinated ligands around the lanthanide ion.[8,9] Another very interesting theoretical approach to the study of magnetic anisotropy of mononuclear lanthanide compounds has been proposed by Baldovì et al. with a different point-charge electrostatic model that leads to magneto-struc-

[a] *Dr. L. Rigamonti, A. Nava, Prof. A. Cornia*
Dipartimento di Scienze Chimiche e Geologiche
Università degli Studi di Modena e Reggio Emilia and
INSTM RU of Modena and Reggio Emilia
via G. Campi 103, 41125 Modena (Italy)
E-mail: acornia@unimore.it

[b] *A. Nava*
Dipartimento di Scienze Fisiche, Informatiche e Matematiche
Università degli Studi di Modena e Reggio Emilia
via G. Campi 213/a, 41125 Modena (Italy)

[c] *Dr. M.-E. Boulon, Prof. R. Sessoli*
Laboratory of Molecular Magnetism (LAMM)
Dipartimento di Chimica "Ugo Schiff"
Università degli Studi di Firenze and INSTM RU of Firenze
via della Lastruccia 3–13, 50019 Sesto Fiorentino (Italy)
E-mail: roberta.sessoli@unifi.it

[d] *Dr. M.-E. Boulon*
Present address: Photon Science Institute
EPSRC School of Chemistry, The University of Manchester
Oxford Road, Manchester M13 9PL (UK)

[e] *Dr. J. Luzon*
Centro Universitario de la Defensa
Academia General Militar, Ctra. de Huesca s/n, 50090 Zaragoza (Spain)

[f] *Dr. J. Luzon*
Instituto de Ciencia de Materiales de Aragón CSIC
Universidad de Zaragoza, C/Pedro Cerbuna 12, 50009 Zaragoza (Spain)

[**] *Ln = Tb, Dy, Ho, Er, Tm, Yb.*

tural correlations.[10] Systematic experimental studies are however still scarce, mainly because it is hard to reproducibly control the coordination environment along the whole lanthanide series: complexes of 1,4,7,10-tetraazacyclododecane-1,4,7,10-tetraacetate ($DOTA^{4-}$) represent a benchmark in this respect.[11]

In this work, we have inserted a lanthanide ion in the threefold-symmetric structure of tetranuclear propeller-like SMM complexes, Fe_3M, as a possible route to enhance their magnetic anisotropy.[4–6] In these robust and chemically-versatile molecules,[12] a tripodal ligand bridges a central metal ion (M^{3+}) to three peripheral high-spin Fe^{3+} centres ($S = 5/2$) positioned at the vertices of a triangle, whereas β-diketonates act as ancillary ligands at the complex periphery. By using 3d metals, derivatives of 2-hydroxymethyl-propane-1,3-diol work well as tripodal ligands (Scheme 1 a). Thus, Fe_4,[13,14] Fe_3Cr,[15,16] and Fe_3V[17] species were isolated, which feature antiferromagnetic Fe–M interactions and ground total spin values ranging from $S = 5$ to 13/2. These molecules conform to either rigorous or idealized D_3 symmetry and display easy-axis anisotropy along the normal to the metal plane. They behave as SMMs, with operating temperatures increasing in the order $Fe_3Cr < Fe_4 < Fe_3V$ and anisotropy barriers reaching up to 21 K.

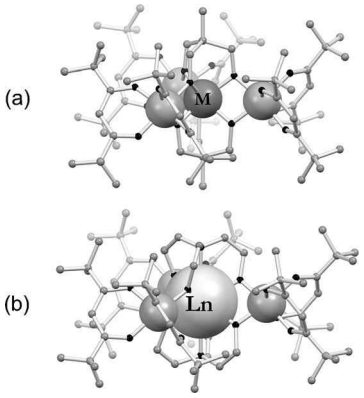

Scheme 1. Schematic representation of: a) **Fe_3M** (M = Fe, Cr, V) SMMs, and b) **Fe_3Ln** propellers. The encapsulation of M^{3+} and Ln^{3+} ions is obtained by two tripodal ligands derived from 2-hydroxymethyl-propane-1,3-diol in (a) and by two tea^{3-} ligands in (b) (O/N = black, C = gray).

Owing to the different size and coordination requirements of 4f versus 3d metal ions, 2-hydroxymethyl-propane-1,3-diol derivatives are unsuitable to encapsulate a lanthanide(III) ion. However, Ln-centered species may be stabilized by triethanolamine (H_3tea, see Scheme 1 b), as shown by the low-yield synthesis of $[Fe_3Ln(tea)_2(acac)_6]$ (Ln = Gd, Dy; Hacac = acetylacetone) reported by Murray and co-workers.[18] By applying the same synthetic strategy used to assemble Fe_3Cr[16] and Fe_3V[17] species we soon found that $[Fe_2(\mu\text{-}OMe)_2(dpm)_4]$ reacts with $[H_3La(tea)_2]$ to give large trigonal crystals of $[Fe_3La(tea)_2(dpm)_6]$ (**Fe_3La**) in high yield (Hdpm = dipivaloylmethane).[19] The whole series of "heavy"-lanthanide(III) complexes **Fe_3Ln** (Ln = Tb, Dy, Ho, Er, Tm, Yb) has now been prepared, and structurally and magnetically characterized. **Fe_3Ln** compounds with Ln = La, Tb–Tm are isomorphous and have crystallographically imposed axial (D_3) symmetry. They therefore provide a unique opportunity to probe different 4f-shell electron distributions while maintaining the same high-symmetry coordination environment.[7] Although single-crystal magnetometry showed that the compounds **Fe_3Dy**, **Fe_3Er**, and **Fe_3Tm** have an easy-axis anisotropy, all derivatives were found to behave as simple paramagnets. Reasons for this are discussed with the help of ab initio theoretical calculations.

Results and Discussion

Synthetic procedures and X-ray crystal structures

The synthesis of **Fe_3Ln** derivatives was accomplished following a two-step procedure, similar to the one that allowed the quantitative incorporation of Cr^{3+}[16] and V^{3+}[17] as central ions. The lanthanide(III) cores $[H_3Ln(tea)_2]$ (Ln = La,[19] Tb, Dy, Ho, Er, Tm, Yb) were first assembled and isolated. Their infrared spectra remain very similar across the whole series (Supporting Information, Figure S1 a). A ν(O–H) signal centered at about 3300 cm^{-1} and covering the 3600–2500 cm^{-1} range is detected and attributed to hydrogen-bond networks. Such broad peak is accompanied by strong ν(C–O) and ν(C–N) bands in the 1100–1000 cm^{-1} range. These spectral features represent a useful fingerprint that allowed us to demonstrate the formation of the desired product when elemental analysis was not feasible, as in the case of $[H_3Tm(tea)_2]$ (see the Experimental Section). Subsequently, by layering a diethyl ether solution of the iron(III) dimer $[Fe_2(\mu\text{-}OMe)_2(dpm)_4]$ over a methanol solution of $[H_3Ln(tea)_2]$, compounds **Fe_3Ln** were obtained as yellow X-ray quality crystals in good to excellent yields (56–79%). The infrared spectrum of **Fe_3Tb** is reported in the Supporting Information (Figure S1b) as representative for the whole series, since the spectra of the six derivatives are practically identical. Bands are narrower than for the $[H_3Ln(tea)_2]$ cores, with characteristic C=O stretching signals of dpm^- ligands in the 1500–1600 cm^{-1} range, and diagnostic shift of ν(C–O) from 1049 cm^{-1} in the iron dimer[19] to about 1080 cm^{-1}.

Similar to the La derivative, compounds with Ln = Tb, Dy, Ho, Er and Tm, crystallize in trigonal space group $R\bar{3}c$ (see the Experimental Section), with six tetranuclear clusters per unit cell and no lattice solvent.[20] Selected interatomic distances and angles are listed in Table 1.

Molecules develop around D_3 symmetry sites. The lanthanide(III) ion lies on the threefold axis and is coplanar with the three crystallographically-equivalent iron(III) ions, which are located on crystallographic twofold axes (see Figure 1 for the representative **Fe_3Er** structure). The lanthanide(III) ion is coordinated by two triply deprotonated triethanolamine molecules, located one above and one below the plane of the metals and lying with their nitrogen atoms on the threefold axis. The tea^{3-} ligands adopt a μ_4 coordination mode and, through their oxygen atoms, bridge the lanthanide to the three iron(III) centers. The molecular size, as measured through the Ln···Fe and Fe···Fe separations, is much larger than in systems entailing a 3d central ion.[14,16,17,21] It declines smoothly in the series, fol-

Table 1. Selected interatomic distances [Å] and angles [°] in compounds **Fe_3Ln**, together with the angular parameters θ, ϕ and γ [°].[a]

	Fe_3La[b]	**Fe_3Tb**	**Fe_3Dy**	**Fe_3Ho**	**Fe_3Er**	**Fe_3Tm**
Ln1-O1	2.4826(16)	2.344(4)	2.323(4)	2.302(3)	2.290(4)	2.277(4)
Ln1-N1	2.758(3)	2.735(7)	2.769(7)	2.801(6)	2.823(8)	2.854(7)
Ln1···Fe1	3.5795(5)	3.4581(14)	3.4398(13)	3.4165(11)	3.4058(14)	3.3919(13)
Fe1···Fe2	6.1999(6)	5.990(3)	5.958(2)	5.9176(19)	5.899(2)	5.875(2)
Fe1-O1	1.9462(18)	1.937(4)	1.940(4)	1.940(3)	1.940(4)	1.940(4)
Fe1-O2	2.0108(19)	2.014(5)	2.010(4)	2.009(4)	2.010(5)	2.009(5)
Fe1-O3	2.0203(19)	2.016(5)	2.012(5)	2.012(4)	2.015(5)	2.015(4)
O1-Ln1-N1 = θ[c]	62.54(4)	63.63(9)	63.66(9)	63.41(8)	63.27(10)	63.19(10)
Ln1-O1-Fe1	107.22(7)	107.42(19)	107.25(16)	106.99(14)	106.94(18)	106.80(18)
O1-Ln1-O1′	62.58(8)	64.64(19)	65.17(18)	65.76(17)	66.0(2)	66.4(2)
O1-Fe1-O1′	82.98(10)	80.6(2)	80.3(2)	80.2(2)	80.1(3)	80.0(3)
ϕ [°][d]	31.23(7)	38.81(16)	39.83(16)	40.19(14)	40.29(16)	40.73(16)
γ [°][e]	62.62(8)	56.17(18)	55.48(18)	55.53(15)	55.64(18)	55.45(18)

[a] Fe1 and Fe2 are related by a threefold rotation around *c*; O1′ is related to O1 by the twofold axis directed along *b*. [b] Data from ref. [19]. [c] Distortion of the LnO_6 polyhedron from octahedral geometry by trigonal compression/elongation. [d] Distortion of the LnO_6 polyhedron from octahedral geometry by trigonal rotation, calculated using formulae in ref. [21] or as the dihedral angle between the planes N1Ln1O1 and N1Ln1O1′. [e] Helical pitch, evaluated as the dihedral angle between the Ln1O1Fe1 and Fe_3Ln planes.

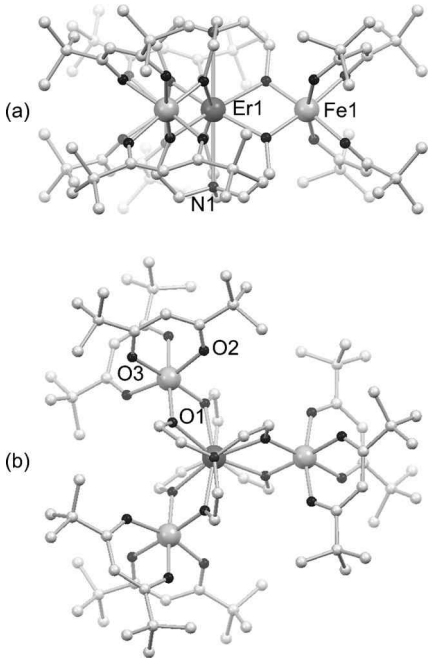

Figure 1. Partially labelled plot of the molecular structure of the *sss* isomer in **Fe_3Er** viewed: a) perpendicular to the threefold molecular axis *c*, and b) along it. Carbon atoms are in light gray, whereas hydrogen atoms are omitted for clarity.

lowing the gradual decrease of Ln ionic radius with increasing atomic number (Table 1).

The coordination environment of the lanthanide can be described as a bicapped distorted trigonal prism, in which the nitrogen atoms give the two caps along the trigonal axis, and the six oxygen atoms occupy the prismatic positions (Figure 2). The tea^{3-} ligands show Ln1–O1 bond lengths ranging from 2.344(4) in **Fe_3Tb** to 2.277(4) Å in **Fe_3Tm**. By contrast, Ln1–N1 distances range from 2.735(7) in **Fe_3Tb** to 2.854(7) Å in **Fe_3Tm**. Thus, Ln1–O1 and Ln1–N1 distances exhibit opposite trends upon contraction of the lanthanide ionic radius along the Tb–Tm series: as atomic number increases, a shortening of Ln1–O1 bonds is accompanied by an elongation of Ln1–N1 distance. Notice that the bigger La^{3+} ion in **Fe_3La**[19] affords La1–O1 = 2.4826(16) Å but La1–N1 = 2.758(3) Å, confirming that the Ln–N distance is not a simple function of lanthanide radius. In $[Fe_3Dy(tea)_2(acac)_6]$, the bond lengths are similar to those of the Dy derivative herein presented, with Dy–O = 2.344(5) and Dy–N = 2.743(5) Å.[18] As expected, in $[Fe_3Gd(tea)_2(acac)_6]$ the Gd–O distance (2.360(6) Å) is larger than in our Tb derivative, whereas Gd–N = 2.740(6) Å.[18]

Neglecting the two nitrogen donors, the O_6 coordination environment of the central ion is the same as in Fe_3M propellers (M = Fe, Cr, V).[14,16,17,21] By consequence, it is of interest to analyze the deviations from perfect octahedral geometry by using the two angles θ and ϕ associated with trigonal compression/elongation and trigonal rotation along the threefold axis (Table 1).[21] The angle θ, which takes the value 54.74° in an octahedron, is here equal to O1-Ln1-N1 and ranges from 62.5 to 63.7°, indicating substantial trigonal compression (for comparison, θ = 54–55° in Fe-centered species containing two tripodal ligands[21]). Such compression is reflected in the short distance between the two opposite triangular faces of the O_6 polyhedron (av.: 2.07 Å) and in the very different O···O separations within each face (av.: 3.58 Å) and between faces (av.: 2.50 and 3.38 Å; the Supporting Information, Table S1). The trigonal rotation angle ϕ, which is 60° in an octahedron and 0° in a trigonal prism, undergoes much larger variations in the series (31.2–40.7°), with the largest and smallest deviations from octahedral geometry observed in the La and Tm derivatives, respectively. The values of θ and ϕ concur to determine a third important angular parameter, namely the helical pitch (γ) of the propeller-like structure, evaluated as the dihedral angle between the Ln1O1Fe1 and Fe_3Ln planes. The helical pitch in **Fe_3La** approaches the lower end of the range covered by tetrairon(III) propellers.[21] However, the heavier lanthanides give much lower γ values (i.e., "weaker" propellers). As found in an isostructural series of Fe_4 derivatives, the approximately

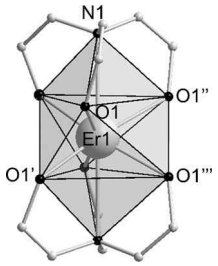

Figure 2. Drawing of the erbium core $[Er(tea)_2]^{3-}$ in **Fe_3Er** with partial atom labeling as used in Table S1 in the Supporting Information.

constant θ causes γ to be mainly triggered by trigonal rotation, so that γ varies inversely with ϕ.[21]

Two dpm$^-$ ligands complete the coordination sphere of each iron(III) ion, giving a distorted octahedral coordination geometry, the major distortion being detected in the O2-Fe1-O2′ angle of about 165° (O2′ is related to O2 by the twofold axis directed along *b*). The dpm$^-$ ligands display major disorder effects, as found in few other Fe_4 propellers.[13,14] In the first arrangement (propeller-like, *p*), the two oxygen donors of dpm$^-$ lie on opposite sides of the molecular plane, whereas in the second arrangement (sandwich-like, *s*) they are found on the same side. The *p* and *s* components have relative occupancies close to 40:60; by contrast, the *p* arrangement is preferred in **Fe_3La**.[19] Assuming independent coordination environments for the three iron(III) ions, the crystal is expected to contain a mixture of *ppp*, *pps*, *ssp*, and *sss* isomers, and their proportions are reported in Table S2 in the Supporting Information. Views of the structures of *ppp* and *sss* isomers are depicted in Figure S2 in the Supporting Information.

Bulk magnetic studies

The temperature dependence of the molar magnetic susceptibility, χ_M, in low fields (1–10 kOe) for compounds **Fe_3Ln** (Ln = Tb, Dy, Ho, Er, Tm and Yb) was measured between 2 and 300 K, and the data are reported in Figure 3 and Figure S3 in the Supporting Information in the form of $\chi_M T$ versus *T* plots. The experimental $\chi_M T$ values at 300 K agree very well with the sum of the Curie constants, *C*, expected for uncoupled high-spin Fe^{3+} ($S = 5/2$, $g = 2.00$) and Ln^{3+} free ions, as reported in Table 2.

Table 2. Magnetic properties of Ln^{3+} ions and **Fe_3Ln** compounds at room temperature.

Ln	Ln^{3+} ground state	g_J	*C* Ln^{3+} [emu K mol^{-1}]	$(\chi_M T)_{calcd}$ **Fe_3Ln**[a] [emu K mol^{-1}]	$(\chi_M T)_{exptl}$ **Fe_3Ln** [emu K mol^{-1}]
Tb	$^7F_6$	3/2	11.84	24.97	25.54
Dy	$^6H_{15/2}$	4/3	14.19	27.32	26.83
Ho	$^5I_8$	5/4	14.08	27.21	26.33
Er	$^4I_{15/2}$	6/5	11.48	24.61	24.84
Tm	$^3H_6$	7/6	7.15	20.28	19.78
Yb	$^2F_{7/2}$	8/7	2.57	15.70	15.37

[a] Curie constant $C(Fe^{3+}) = 4.38$ emu K mol^{-1}.

For derivatives **Fe_3Tb**, **Fe_3Dy**, and **Fe_3Ho**, the value remains constant upon cooling to around 25 K, and then it increases rapidly to reach 45.73, 41.97, and 32.82 emu K mol^{-1}, respectively, indicating a weak ferromagnetic interaction between the lanthanide and the iron ions. For comparison, a similar behavior was also reported for compounds $[Fe_3Ln(tea)_2(acac)_6]$ (Ln = Gd, Dy); for the gadolinium derivative a coupling constant of 0.73 cm^{-1} was obtained by fitting experimental data to a Heisenberg exchange Hamiltonian ("$-2J$" formalism).[18] Compound **Fe_3Er** shows an initial slow decline of the $\chi_M T$ product upon cooling, followed by an increase below 25 K towards

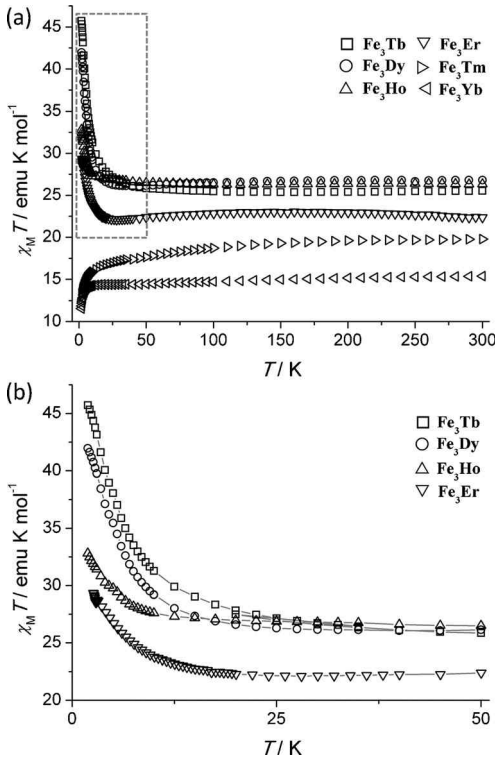

Figure 3. a) Temperature dependence of the $\chi_M T$ product for **Fe_3Ln** (Ln = Tb–Yb) in the 2–300 K range. b) Magnified view of the gray dashed box in (a) for compounds with Ln = Tb–Er; gray lines are a guide for the eye.

29.34 emu K mol^{-1} at 2 K. The $\chi_M T$ product of **Fe_3Tm** and **Fe_3Yb** decreases slowly and reaches 12.75 and 11.30 emu K mol^{-1}, respectively, at 2 K. Such behavior presumably reflects either weak antiferromagnetic couplings or the depopulation of sublevels of the ground *J* multiplet split by the CF.

The field dependence of the isothermal magnetization, M_M, at low temperatures for compounds **Fe_3Ln** is shown in Figure S3 in the Supporting Information as M_M versus H/T plots. The pronounced nesting of the curves hints to deviations from Brillouin function and is consistent with the presence of magnetic anisotropy and/or intramolecular exchange interactions.

The magnetization dynamics of compounds **Fe_3Ln** was then investigated by alternating current (AC) susceptibility measurements in zero and 1- or 2 kOe applied static fields to look for SMM behavior. The analysis was performed as a function of both temperature (down to 1.8 K) and frequency of the oscillating field ($\nu = 10$–$10\,000$ Hz), and the results are reported in Figure S4 in the Supporting Information. In all conditions explored, all **Fe_3Ln** derivatives (from Tb to Yb) show no frequency dependent maxima in the χ''_M versus *T* plots, and therefore behave as simple paramagnets, even if a substantial axial anisotropy is expected.

Single-crystal magnetic studies on Fe_3Dy, Fe_3Ho, Fe_3Er, and Fe_3Tm derivatives

To gain information on magnetic anisotropy, the angular dependence of the magnetization was measured following a

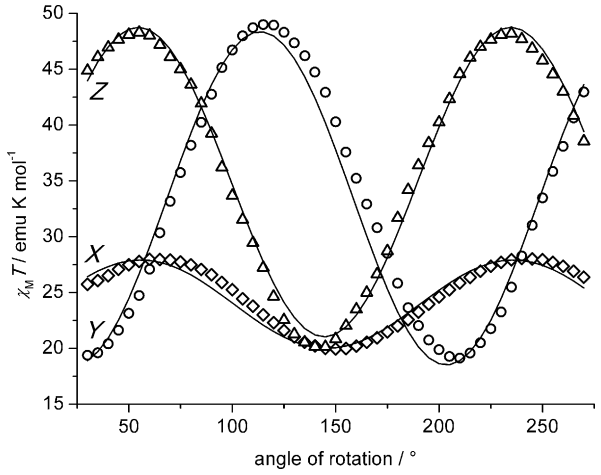

Figure 4. Angular dependence of the $\chi_M T$ product for **Fe_3Er** at $T = 2$ K and $H = 1.0$ kOe for the rotations along the X (◇), Y (○), and Z (△) axes of the laboratory reference frame. The black solid lines represent best-fit curves (see text).

procedure established by our group and requiring no face indexing.[22] Briefly, a single crystal of **Fe_3Ln** was fixed on a face of a millimetric Teflon cube, whose faces define the laboratory *XYZ* reference system. The cube faces were indexed in the reference frame of the crystal with non-integer Miller indices (see Experimental Section and the Supporting Information, Table S3, for further details). The system cube + crystal was then mounted on a horizontal rotator and placed in the SQUID magnetometer with a vertical magnetic field. Unfortunately, crystals of **Fe_3Tb** were too small to give a reliable set of data, whereas crystals of **Fe_3Yb** were not analyzed because major difficulties were encountered in the structure refinement.[20] The outcomes of three isothermal ($T = 2$ K) rotations along *X*, *Y*, and *Z* for **Fe_3Er** are reported as plots of $\chi_M T$ against the rotation angle in Figure 4 (similar measurements for **Fe_3Dy**, **Fe_3Ho**, and **Fe_3Tm** can be found in the Supporting Information, Figure S5).

Table 3. Principal components of the diagonalized susceptibility tensors χ derived from single-crystal angle-resolved magnetic measurements, and orientation of the obtained anisotropy direction with respect to the crystallographic *c* axis for **Fe_3Dy**, **Fe_3Er**, and **Fe_3Tm**.

	Fe_3Dy	**Fe_3Er**	**Fe_3Tm**
χ_1 [emu mol^{-1}]	9.31(9)	9.240(3)	5.4602(10)
χ_2 [emu mol^{-1}]	10.057(2)	10.5865(19)	5.8275(13)
χ_3 [emu mol^{-1}]	43.36(4)	26.33(8)	8.7758(13)
χ^2	29.447	18.435	22.558
$\cos\delta_c$	0.99953(8)	0.99952(17)	0.996812(1)
pictorial ellipsoid			

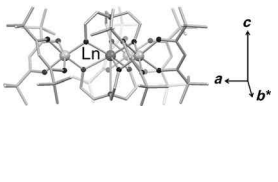

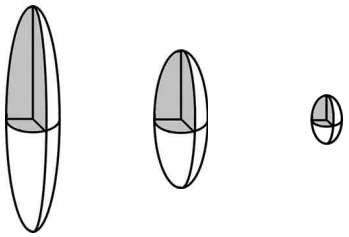

By exploiting the tensorial character of the susceptibility, and considering that we measure the component of the magnetization along the applied field, the experimental data were fitted to Equation (1):

$$\chi^{rot\gamma}(\sigma) = \chi_{\alpha\alpha}\cos^2\sigma + \chi_{\beta\beta}\sin^2\sigma + 2\chi_{\alpha\beta}\cos\sigma\sin\sigma \qquad (1)$$

with cyclic permutation of the α, β, and γ indices over the *XYZ* reference frame. Here, σ is the angle between the magnetic field and the α axis. The susceptibility tensor χ was then diagonalized to provide its principal components (χ_1, χ_2, χ_3) and its orientation, reported in Table 3 in the *ortho*-normalized cell *a*, *b**, *c*. No axial symmetry of the susceptibility tensor was assumed during the fitting process, thus resulting in different in-plane χ_1 and χ_2 values; this non-axial response thus reflects the experimental uncertainty of the technique. In the case of **Fe_3Ho**, a meaningful fit was not possible due to the almost isotropic magnetic behavior of this compound. In the three remaining derivatives, the χ_3 component is dominant and magnetic anisotropy is of the easy-axis type; it decreases in the order **Fe_3Dy** > **Fe_3Er** > **Fe_3Tm**, as pictorially represented by the ellipsoids in Table 3. Since $\cos\delta_c \approx 1$, where δ_c is the angle between *c* and χ_3 direction, the easy axis lies close to the threefold crystal axis; deviations (1.8° in **Fe_3Dy** and **Fe_3Er**; 4.6° in **Fe_3Tm**) reflect the expected accuracy in crystal alignment.

Ab initio and theoretical calculations

To better understand the magnetic properties of these systems and, in particular, to explain the absence of SMM behavior, two different kinds of ab initio quantum chemistry calculations were performed on the compounds for which structural data are available (Ln = Tb–Tm). First, relativistic DFT calculations were carried out on Fe^{3+} ions to determine their magnetic anisotropy. Second, relativistic quantum chemistry calculations were performed for Ln^{3+} ions to establish the energy level structure for the $^{2S+1}L_J$ ground multiplets, the composition of the corresponding wave functions, and the magnetic anisotropy. The results of these calculations were used for fitting experimental bulk magnetic susceptibility data applying an exchange Hamiltonian model to estimate the Fe–Ln and Fe–Fe exchange coupling constants. The magnetic anisotropy of **Fe_3Ln** compounds was then modelled with the same Hamiltonian and compared with the experimental one, when available.

The relativistic DFT calculations on Fe^{3+} ions were conducted with the quantum chemistry ORCA package.[23] By using the X-ray molecular structure of **Fe_3Dy** as a model (see the Experimental Section for details), an easy-plane magnetic an-

isotropy was obtained for Fe^{3+} ions, with $D/k_B = +1.04$ K ($+0.723$ cm^{-1}). This value is fully comparable to that found for **Fe_3La**[19] using experimental torque magnetometry data ($D = +0.989(9)$ cm^{-1}) and DFT calculations ($+1.094$ cm^{-1}). The ab initio magnetic hard axis forms an angle of 73° with the threefold molecular axis and is thus close to the Fe_3Ln plane. It is also closely coincident with O2-Fe1-O2′ direction, that is, one of the axes of the FeO_6 octahedron (Supporting Information, Figure S6), and almost perpendicular to the Fe–Ln direction. Notice that, due to symmetry reasons, the latter must coincide with one of the principal directions of the anisotropy tensor. However, small deviations may be expected in the DFT calculations as the wave function is not symmetry restricted. Since Fe^{3+} magnetic hard axis is strongly related to O2-Fe1-O2′ direction, and the environment around the iron ions is very similar for all compounds, in the subsequent calculations we have set the Fe^{3+} hard axis at 73° from the threefold molecular axis and perpendicular to the Fe–Ln direction.

The relativistic quantum chemistry calculations on the magnetic anisotropy of the Ln^{3+} ions were performed by using the CASPT2/RASSI-SO method[24] as implemented in the MOLCAS 7.8 package.[25] To this purpose, iron(III) was replaced with diamagnetic gallium(III). The calculations were performed on *ppp* isomers, in which the lanthanide ions reside in an axially symmetric (D_3) environment that is most favorable for SMM behavior. The computed energies of the ground and first two excited states for Ln^{3+} ions are given in Table 4, whereas the full energy level structures of the $^{2S+1}L_J$ ground multiplets are shown in Table S4 in the Supporting Information. Knowing the electronic states and their energies, a straightforward way to study the Ln^{3+} magnetic anisotropy is by computing the main values of the gyromagnetic tensor. Here, it is interesting to remark that, due to the D_3 symmetry around the Ln^{3+} ions, the gyromagnetic tensor should be axial, with one of the principal components (g_z) along the threefold axis z and isotropic in-plane values (i.e., $g_x = g_y$). The g-tensor is commonly calculated using a pseudo-spin $S = 1/2$ formalism, which is only applicable to doublet states.[26] We thus opted for a different approach that allows to treat ions with singlet ground states as well. The g-tensor herein provided is the effective gyromagnetic tensor required for an $S = 1/2$ state to reproduce the ab initio anisotropic susceptibility tensor at a given temperature. These effective gyromagnetic factors at $T = 2$ K are shown in Table 4.

A well-isolated ground doublet state and a strong uniaxial anisotropy of the gyromagnetic tensor are two of the main requirements for an Ln^{3+} complex to display SMM behavior. From the data in Table 4, it is apparent that none of the herein studied **Fe_3Ln** compounds meets such requirements. Tb^{3+} and Tm^{3+} complexes have a singlet ground state, whereas all other compounds have ground Kramers doublets but do not possess strong uniaxial anisotropy. The ground doublet state is therefore a mixture of $|m_J>$ states, which favors the quantum tunneling of the magnetization and prevents the observation of a directionally-bistable magnetic moment at low temperature.

Table 4. Computed energies of the ground (E_0) and the first two excited states (E_1, E_2) for the Ln^{3+} ions, and the effective gyromagnetic factors along the threefold molecular axis (g_z) and in the xy plane ($g_{x,y}$) at $T = 2$ K; (×2) after the energy values indicates a doublet state.

	Tb^{3+}	Dy^{3+}	Ho^{3+}	Er^{3+}	Tm^{3+}
E_0 [K]	0.0	0.0 (×2)	0.0 (×2)	0.0 (×2)	0.0
E_1 [K]	27.6	56.6 (×2)	20.4	40.6 (×2)	9.8
E_2 [K]	48.1 (×2)	89.9 (×2)	62.1 (×2)	122.6 (×2)	332.3 (×2)
g_z	3.94	9.85	7.62	5.72	6.59
$g_{x,y}$	2.39	4.51	4.36	7.76	0.37

Comparison with experimental data requires taking into account also the Fe–Ln and Fe–Fe intramolecular exchange interactions. As stated previously, the ab initio results for Fe^{3+} and Ln^{3+} ions can be used to fit experimental magnetic data through Hamiltonian:

$$H = \sum_{i=1}^{3} DS_{z_i}^2 + H_{CF}(\mathrm{Ln}) - J_1 \sum_{i,j=1,2,3}^{i<j} \vec{S}_i \cdot \vec{S}_j - J_2 \sum_{i=1}^{3} \vec{S}_i \cdot \vec{J} - g_e \mu_B \sum_{i=1}^{3} \vec{S}_i \cdot \vec{B} - g_J \mu_B \vec{J} \cdot \vec{B} \quad (2)$$

In Equation (2), the first term accounts for Fe^{3+} anisotropy along the individual z_i hard axes, whereas the second term describes Ln^{3+} anisotropy. The third and fourth terms introduce Heisenberg exchange interactions among Fe^{3+} ions (J_1) and between Fe^{3+} and Ln^{3+} ions (J_2), respectively. Finally, the last two terms account for Zeeman splitting in a magnetic field $\vec{B}$. Statistical physics methods can be applied to this Hamiltonian to obtain the magnetic properties of **Fe_3Ln**. For doing so, the directions of the non-collinear hard axes for the three Fe^{3+} ions and the crystal field on Ln^{3+} ion were taken from ab initio results, whereas D, J_1, and J_2 were treated as adjustable parameters.

The fit of the powder $\chi_M T$ measurements for **Fe_3La**[19] with the above Hamiltonian, in which $J_2 = 0$ due to the diamagnetic lanthanum(III) core, resulted in $D = +0.80$ K and $J_1 = -0.10$ K. This D value is lower than the one obtained in ref. [19]; reasons have to be traced back to the non-coincidence of the two Hamiltonian models; in particular, the Fe^{3+} hard axis is taken to lie on the metal plane in **Fe_3La**,[19] whereas it deviates by about 17° from the Fe_3Ln plane in the present model. Furthermore, there is a large correlation between D and J_1 parameters. Next, the experimental powder $\chi_M T$ values for **Fe_3Ln** (Ln = Tb–Tm) were analyzed using J_1 and J_2 as adjustable parameters while fixing $D = +0.80$ K to reduce the number of variables. We decided to use this experimental value instead of the DFT estimate because it can be considered more reliable. Notice, however, that the D parameter has only a small influence on the overall anisotropy of **Fe_3Ln** (Ln = Tb–Tm).

For **Fe_3Tb** and **Fe_3Tm** such fits resulted in unrealistically large ferromagnetic J_1 values, whereas interaction strengths of similar magnitude are expected in all the compounds. Therefore, data for **Fe_3Tb** and **Fe_3Tm** were fitted by fixing J_1 to -0.10 K and leaving only J_2 as a variable parameter. The results obtained with this approach are gathered in Figure S3 in the Supporting Information, whereas the best-fit values of J_1 and J_2 are given in Table 5. The agreement between experimental and calculated data is satisfactory for all compounds except **Fe_3Tb** and **Fe_3Tm**, in which J_1 was fixed. For these two, the

Table 5. Exchange coupling constants J_1 and J_2, calculated from the fit of the powder $\chi_M T$ measurements.[a]

	J_1 [K]	J_2 [K]	$(\chi_M)_{x,y}$ [emu mol^{-1}]	$(\chi_M)_z$ [emu mol^{-1}]	$(\chi_M)_z/(\chi_M)_{x,y}$ calcd	expt[b]
Fe_3Tb	−0.10 (F)	0.87	8.37	49.65	5.93	–
Fe_3Dy	0.05	0.34	9.55	45.90	4.81	4.47
Fe_3Ho	−0.18	0.43	15.74	19.81	1.26	isotropic
Fe_3Er	−0.08	0.36	18.22	11.67	0.64	2.66
Fe_3Tm	−0.10 (F)	−0.02	4.83	7.34	1.52	1.55

[a] Principal values of χ_M at $T = 2$ K computed along the trigonal axis (z) and in the xy plane are also given, together with their theoretical and experimental ratio. (F) indicates that the parameter was held fixed in the fit. [b] The values of $\chi_{1,2}$ in Table 3 were averaged to obtain $(\chi_M)_{x,y}$.

worst matching appears in the 10–75 K region, and a possible explanation for such disagreement is that the energies of the lowest states are not well reproduced by the ab initio calculations.

Based on the best-fit sets of Hamiltonian parameters, the χ_M values at 2 K were calculated along the trigonal axis (z) and in the xy plane and compared with the experimental ones (Table 5).

Except for **Fe_3Er**, there is a good agreement between the experimental and the theoretical magnetic anisotropies for all compounds. This suggests that our ab initio evaluation of magnetic anisotropy is reliable and the proposed explanation for the absence of SMM behavior is realistic. For the erbium derivative, experimental data indicate easy-axis anisotropy, whereas the calculated anisotropy is of the easy-plane type. The same trend was encountered in the [Ln(dota)] series,[11] suggesting that relativistic ab initio results on Er^{3+} ions must be taken with care. However, in the present case a source of disagreement may also be the use of a fully isotropic exchange Hamiltonian.

Finally, it is important to stress that the magnetic anisotropies of the Ln^{3+} ion and of the whole **Fe_3Ln** molecule are not directly correlated. Molecular magnetic anisotropy is crucially dependent on the interplay between local magnetic anisotropies at lanthanide(III) and iron(III) sites and intramolecular magnetic interactions, even when the latter are assumed to be isotropic. For instance, the single-ion magnetic anisotropy is larger for Tm^{3+} than for Dy^{3+} ion, but **Fe_3Tm** has a much lower magnetic anisotropy than **Fe_3Dy**.

Conclusion

In an attempt to enhance the magnetic anisotropy of Fe_4 SMMs by selective substitution of the central iron(III) ion with a lanthanide(III), while advancing the work by Chilton et al. on $acac^-$ analogues,[18] the series of **Fe_3Ln** complexes was prepared with Ln = Tb–Yb. Although angle-resolved single crystal susceptibility measurements highlight the presence of easy-axis anisotropy in the case of **Fe_3Dy**, **Fe_3Er**, and **Fe_3Tm**, all synthesized compounds behave as paramagnets and do not show slow magnetic relaxation at 1.8 K with AC field frequencies up to 10000 Hz.

Theoretical calculations have shown that lanthanides displaying a doublet ground state (Dy, Ho, Er) also exhibit extensive admixture of m_J states, which prevents SMM behavior. The presence of two purely axial nitrogen donors together with six oxygen atoms arranged at the vertices of a compressed and trigonally distorted octahedron gives rise to a coordination geometry probably intermediate between axial and equatorial in Long's model.[7] The former is typical of phthalocyaninates[5a,7,27] or polyoxometalates,[28] whereas an equatorial environment is produced by Cp/COT ligands[7,29] but also by properly arranged monodentate species, as in $Er[N(SiMe_3)_2]_3$.[30] Our systematic study then shows that lanthanide(III) coordination in **Fe_3Ln**, though uniaxial, can be considered unsuitable to stabilize pairs of virtually pure m_J states with large $|m_J|$ both for "oblate" and "prolate" 4f ions.

Experimental Section

Materials and methods

All chemicals were of reagent grade and were used as received. Toluene was absolute over molecular sieves ($H_2O \leq 0.005\,\%$). Isopropanol was distilled over CaO and stored over 3 Å molecular sieves, methanol was distilled over magnesium methoxide and stored over 3 Å molecular sieves, and diethyl ether was predried over $CaCl_2$ overnight and distilled from sodium-benzophenone under N_2 before use. Elemental analyses were carried out on a Carlo Erba EA1110 CHNS-O automatic analyzer. Infrared spectra were recorded as KBr disks using a Jasco FTIR-4200 spectrophotometer with a 2 cm^{-1} resolution. $[Ln(OAc)_3]$ (Ln = Tb, Dy, Ho, Er, Tm, Yb)[31] and $[Fe_2(\mu\text{-}OMe)_2(dpm)_4]$[14] were synthesized as reported in the literature.

Syntheses

Synthesis of $[H_3Ln(tea)_2]$:[19] The reaction was performed under dinitrogen inert atmosphere with oven-dried glassware. Sodium in small pieces was added to a suspension of $[Ln(OAc)_3]$ in toluene (20 mL) and isopropanol (2 mL) and the resulting mixture was heated at reflux for 4 h. A white precipitate (NaOAc) formed upon cooling; the colorless solution of $[Ln(O\mathit{i}Pr)_3]$ was syringed to a second flask under dinitrogen flow. The solid was further treated with toluene (2 × 5 mL), and all the organic phases were combined. A solution of H_3tea in isopropanol (3 mL) was added and the reaction mixture was left under stirring at room temperature for 24 h; it was then concentrated under vacuum until a white gelatinous precipitate was obtained; the product was collected, washed with isopropanol and dried in vacuum.

$[H_3Tb(tea)_2]$: Prepared from $[Tb(OAc)_3]$ (0.3421 g, 1.018 mmol), sodium (0.0762 g, 3.31 mmol), and H_3tea (0.3016 g, 2.022 mmol). Yield: 0.1943 g (42.31 %); elemental analysis calcd (%) for $C_{12}H_{27}N_2O_6Tb$ (454.28): C 31.73, H 5.99, N 6.17; found: C 31.94, H 6.20, N 5.98.

$[H_3Dy(tea)_2]$: Prepared from $[Dy(OAc)_3]$ (0.6778 g, 1.996 mmol), sodium (0.1488 g, 6.472 mmol), and H_3tea (0.6036 g, 4.044 mmol). Yield: 0.4163 g (45.46 %); elemental analysis calcd (%) for $C_{12}H_{27}DyN_2O_6$ (457.86): C 31.48, H 5.94, N 6.12; found: C 31.27, H 5.83, N 6.07.

$[H_3Ho(tea)_2]$: Prepared from $[Ho(OAc)_3]$ (0.3657 g, 1.069 mmol), sodium (0.0793 g, 3.45 mmol), and H_3tea (0.3324 g, 2.228 mmol). Yield: 0.4191 g (85.18 %). Elemental analysis calcd (%) for

$C_{12}H_{27}HoN_2O_6{\cdot}0.15C_7H_8$ (474.10): C 33.06, H 6.00, N 5.91; found: C 33.35, H 6.16, N 5.94.

$[H_3Er(tea)_2]$: Prepared from $[Er(OAc)_3]$ (0.4302 g, 1.249 mmol), sodium (0.1045 g, 4.545 mmol), and H_3tea (0.3871 g, 2.595 mmol). Yield: 0.4187 g (68.46%); elemental analysis calcd (%) for $C_{12}H_{27}ErN_2O_6{\cdot}1.5\,H_2O$ (489.64): C 29.44, H 6.18, N 5.72; found: C 29.40, H 6.18, N 6.04.

$[H_3Tm(tea)_2]$: Prepared from $[Tm(OAc)_3]$ (0.4131 g, 1.194 mmol), sodium (0.1082 g, 4.706 mmol), and H_3tea (0.3800 g, 2.547 mmol). Yield: 0.3755 g (67.73%). The gelatinous solid was not suitable for proper elemental analysis.

$[H_3Yb(tea)_2]$: Prepared from $[Yb(OAc)_3]$ (0.3010 g, 0.8596 mmol), sodium (0.0807 g, 3.51 mmol), and H_3tea (0.2763 g, 1.852 mmol). Yield: 0.1350 g (30.59%); elemental analysis calcd (%) for $C_{12}H_{27}N_2O_6Yb{\cdot}2.5H_2O$ (513.43): C 28.07, H 6.28, N 5.46; found: C 27.96, H 6.16, N 5.16.

Synthesis of $[Fe_3Ln(tea)_2(dpm)_6]$ (Fe_3Ln):[19] A solution of $[Fe_2(\mu\text{-}OMe)_2(dpm)_4]$ in diethyl ether (10 mL) was layered over a solution of $[H_3Ln(tea)_2]$ in methanol (5 mL) in a cylindrical flask, with *n*-hexane buffer (1 mL) between the two layers. The system was left under slow diffusion over a period of 2–4 weeks during which the formation of yellow crystals suitable for X-ray diffraction was observed. Once the diffusion was complete, the crystalline product was collected by filtration and dried in vacuum.

Fe_3Tb: Prepared from $[Fe_2(\mu\text{-}OMe)_2(dpm)_4]$ (0.0749 g, 0.0826 mmol) and $[H_3Tb(tea)_2]$ (0.0251 g, 0.0552 mmol). Yield: 0.0601 g (63.5%); elemental analysis calcd (%) for $C_{78}H_{138}Fe_3N_2O_{18}Tb$ (1718.37): C 54.52, H 8.09, N 1.63; found: C 54.55, H 8.25, N 1.77.

Fe_3Dy: Prepared from $[Fe_2(\mu\text{-}OMe)_2(dpm)_4]$ (0.0610 g, 0.0673 mmol) and $[H_3Dy(tea)_2]$ (0.0239 g, 0.0522 mmol). Yield: 0.0613 g (79.3%); elemental analysis calcd (%) for $C_{78}H_{138}DyFe_3N_2O_{18}$ (1721.95): C 54.40, H 8.08, N 1.63; found: C 54.38, H 8.31, N 1.75.

Fe_3Ho: Prepared from $[Fe_2(\mu\text{-}OMe)_2(dpm)_4]$ (0.0427 g, 0.0471 mmol) and $[H_3Ho(tea)_2]$ (0.0145 g, 0.0315 mmol). Yield: 0.0307 g (56.7%); elemental analysis calcd (%) for $C_{78}H_{138}Fe_3HoN_2O_{18}$ (1724.38): C 54.33, H 8.07, N 1.62; found: C 54.39, H 8.27, N 1.74.

Fe_3Er: Prepared from $[Fe_2(\mu\text{-}OMe)_2(dpm)_4]$ (0.0552 g, 0.0609 mmol) and $[H_3Er(tea)_2]$ (0.0210 g, 0.0454 mmol). Yield: 0.0510 g (72.7%); elemental analysis calcd (%) for $C_{78}H_{138}ErFe_3N_2O_{18}$ (1726.71): C 54.25, H 8.06, N 1.62; found: C 54.07, H 8.16, N 1.59.

Fe_3Tm: Prepared from $[Fe_2(\mu\text{-}OMe)_2(dpm)_4]$ (0.0647 g, 0.0713 mmol) and $[H_3Tm(tea)_2]$ (0.0268 g, 0.0577 mmol). Yield: 0.0465 g (56.6%); elemental analysis calcd (%) for $C_{78}H_{138}Fe_3N_2O_{18}Tm$ (1728.38): C 54.20, H 8.05, N 1.62; found: C 53.93, H 8.15, N 1.62.

Fe_3Yb: Prepared from $[Fe_2(\mu\text{-}OMe)_2(dpm)_4]$ (0.0547 g, 0.0603 mmol) and $[H_3Yb(tea)_2]$ (0.0187 g, 0.0399 mmol). Yield: 0.0486 g (70.3%); elemental analysis calcd (%) for $C_{78}H_{138}Fe_3N_2O_{18}Yb$ (1732.51): C 54.07, H 8.03, N 1.62; found: C 54.25, H 8.29, N 1.54.

X-ray crystallography

Single-crystal X-ray diffraction studies on **Fe_3Ln** compounds[20] were carried out at 140(2) K with a four-circle Bruker X8-APEX diffractometer equipped with a $Mo_{K\alpha}$ generator ($\lambda = 0.71073$ Å), an area detector and a Kryo-Flex cryostat, and controlled by Bruker-Nonius X8-APEX software. Crystallographic data and refinement parameters are reported in Table 6. The structures were solved by direct methods using the SIR92[32] program and the full-matrix least-squares refinement on F_o^2 was performed using the SHELX-97[33] program; both programs are implemented in the WINGX[34] v1.80.05 package. The programs Mercury 3.5.1[35] and Diamond 3.1[36] were used for graphics. For all compounds, two different arrangements of dpm^- ligands coordinated to Fe were observed, with resolved disorder on carbon but not on oxygen atoms. In the first one (propeller-like, *p*) the two oxygen donors of dpm^- lie on opposite sides of the molecular plane (oxygen atoms A); in the second one (sandwich-like, *s*) they lie on the same side of the molecular plane (oxygen atoms B). Complementary occupancy factors were assigned to the carbon and oxygen atoms of *p* and *s*, resulting in the highest occupancy for *s* (the Supporting Information, Table S2). Furthermore, oxygen atoms A and B were constrained to have the same coordinates (EXYZ instruction) and the same thermal parameters (EADP instruction). The C–O distances of the sandwich part were restrained to be (1.266 ± 0.008) Å. The carbon skeleton of the dpm^- propeller component was restrained to have the same geometry as the sandwich component within 0.01 Å for 1,2 distances and 0.02 Å for 1,3 distances. The C–C distances within each *t*Bu group of the sandwich part were also restrained to be similar within 0.01 Å. All non-hydrogen atoms were refined anisotropically. Because of the extensive overlap between the two components, the methyl carbons of *t*Bu groups in both *p* and *s* arrange-

Table 6. Crystallographic data and refinement parameters for **Fe_3Ln**.[20]

	Fe_3Tb	Fe_3Dy	Fe_3Ho	Fe_3Er	Fe_3Tm
formula	$C_{78}H_{138}Fe_3N_2O_{18}Tb$	$C_{78}H_{138}DyFe_3N_2O_{18}$	$C_{78}H_{138}Fe_3HoN_2O_{18}$	$C_{78}H_{138}ErFe_3N_2O_{18}$	$C_{78}H_{138}Fe_3N_2O_{18}Tm$
M_r	1718.37	1721.95	1724.38	1726.71	1728.38
crystal system	trigonal	trigonal	trigonal	trigonal	trigonal
space group	$R\bar{3}c$ (no. 167)	$R\bar{3}c$ (no. 167)	$R\bar{3}c$ (no. 167)	$R\bar{3}c$ (no. 167)	$R\bar{3}c$ (no. 167)
$a = b$ [Å]	16.4841(2)	16.4739(3)	16.4568(3)	16.4626(2)	16.4451(2)
c [Å]	57.0970(18)	57.1558(17)	57.1691(23)	57.1102(14)	57.1671(11)
V [Å^3]	13436.1(5)	13433.3(5)	13408.6(6)	13404.2(4)	13389.0(3)
Z	6	6	6	6	6
ρ_{calcd} [g cm^{-3}]	1.274	1.277	1.281	1.283	1.286
μ [mm^{-1}]	1.316	1.361	1.413	1.467	1.523
crystal size [mm^3]	0.29×0.27×0.25	0.33×0.27×0.21	0.43×0.27×0.26	0.46×0.36×0.18	0.41×0.33×0.18
$2\theta_{max}$ [°]	58.00	58.04	58.02	58.02	58.00
collected/indep reflns	31751/3971	34328/3953	31970/3963	49152/3970	31865/3956
R_{int}	0.0378	0.0375	0.0300	0.0333	0.0346
restraints/parameters	281/255	293/255	293/255	293/255	293/255
R_1, wR_2 ($I > 2\sigma(I)$)	0.0751, 0.1682	0.0761, 0.1665	0.0656, 0.1560	0.0884, 0.1688	0.0863, 0.1723
R_1, wR_2 (all data)	0.1202, 0.1881	0.1048, 0.1788	0.1028, 0.1735	0.1186, 0.1800	0.1186, 0.1868
GoF	1.213	1.212	1.146	1.240	1.163

ments had to be restrained to approximate isotropic behavior within 0.04 Å^2. Furthermore, all the other carbon atoms were also restrained to approximate isotropic behavior within 0.02 Å^2. All carbon atoms, except for the tea^{3-} ones, were restrained to have similar thermal ellipsoid vibrations within 0.02 Å^2. Hydrogen atoms were added in idealized positions and assigned isotropic displacement parameters constrained to those of the attached carbon atoms.

CCDC 1050650, 1050651, 1050652, 1050653 and 1050654 contain the supplementary crystallographic data for this paper. These data are provided free of charge by The Cambridge Crystallographic Data Centre.

Magnetic measurements

DC magnetic data were recorded using a Quantum Design MPMS SQUID magnetometer. Magnetic susceptibilities were measured on 20.57, 16.79, 15.40, 11.60, 14.01, and 15.90 mg powder samples of **Fe_3Ln** (Ln = Tb, Dy, Ho, Er, Tm, Yb, respectively), packed in a pressed Teflon pellet with applied fields of 1 kOe from 1.9 to 35 K and of 10 kOe from 35 to 300 K. Isothermal magnetization data were also registered between 1.9 and 5 K in fields up to 50 kOe. Data reduction was carried out by using $-944.3\ 10^{-6}$ emu mol^{-1} as diamagnetic contribution for all compounds, estimated from the Pascal's constants.[37] AC susceptibility of the **Fe_3Ln** series was recorded on the same samples using the aforementioned SQUID magnetometer (Tb, Dy, Ho) or a Quantum Design PPMS susceptometer (Er, Tm, Yb).

Single-crystal angle-resolved magnetic studies

A crystal of each compound **Fe_3Ln** (Ln = Dy, Ho, Er and Tm), about $0.2\times0.4\times0.4$ mm^3 in size, was fixed on a Teflon cube ($\approx$20 mg) with Apiezon grease and the ensemble was mounted on a goniometer head. The faces of the cube, whose normals define the *XYZ* orthogonal reference frame, were indexed at room temperature with non-integer Miller indices in the **Fe_3Ln** unit cell reference frame, using an Oxford Diffraction Xcalibur3 four-circle X-ray diffractometer. The composition of the *XYZ* directions in the *hkl* crystal reference is reported in Table S3 in the Supporting Information. Three orthogonal rotations around *X*, *Y*, and *Z* axes were then performed using a Quantum Design horizontal sample rotator to measure the angular dependence of the magnetic susceptibility (assumed to coincide with the *M*/*H* ratio at *H* = 1.0 kOe). Data were corrected for the diamagnetic contribution of the cube sample holder and rotator, and fitted using a home-written program. As sample mass cannot be directly measured with the required accuracy, susceptibility data were properly scaled by comparing the χ_M value obtained by powder measurements at 2 K with the orientationally averaged magnetic susceptibility resulting from single-crystal measurements at the same temperature.

Computational and theoretical details

The DFT calculations for obtaining the magnetic anisotropy, including the main anisotropy axes, the uniaxial *D* parameter and the *g*-factors, were performed with the quantum chemistry package ORCA.[23] The spin–orbit coupling effects were treated within the spin–orbit mean-field approximation (SOMF).[38] The calculations were performed on a quantum cluster around one of the Fe^{3+} ions. The geometry was taken from the X-ray crystal structure of **Fe_3Dy**, replacing Dy^{3+} with Y^{3+} and the other two Fe^{3+} ions with diamagnetic Ga^{3+} ions in order to have only one magnetic center. Ga^{3+} and high-spin Fe^{3+} ions have similar radius and coordination chemistry. In addition, dpm$^-$ ligands coordinated to Ga^{3+} were replaced by OH$^-$ groups (Supporting Information, Figure S6) to reduce the computational time. The employed basis-set was the Ahlrichs Def-TZVP[39] for all the atoms and the exchange-correlation functional was the BP86 one.[40]

Post-Hartree–Fock ab initio calculations were carried out using the CASSCF/RASSI-SO method[24] as implemented in the MOLCAS 7.8 package.[25] Computations were performed on **Fe_3Ln** molecules from their X-ray structures for each lanthanide derivative, in which the dpm$^-$ ligands ($C_{11}H_{19}O_2$) linked to Fe^{3+} ions were replaced by acac$^-$ ligands ($C_5H_7O_2$) to reduce the computational time, but preserving the reliability of the calculations. In addition, Fe^{3+} ions were replaced by Ga^{3+} ions to reduce the active space. All the atoms were represented by a basis set of atomic natural orbitals from the ANO-RCC library, as implemented in the MOLCAS quantum-chemistry package. The following contractions were used: [8s7p4d3f2g1h] for lanthanide ions, [6s5p3d] for Ga^{3+} ions, [4s3p1d] for O, N, and C atoms in the first and second shell of atoms around the lanthanide ions, [3s2p] for all the other C and O atoms and [3s] for H atoms. The CASSCF active space consisted of the lanthanide 4f orbitals.

The MOLCAS package does not allow the treatment of the D_3 symmetry around the Ln^{3+} ions and therefore the computed electronic states are not symmetry adapted. However, we recovered symmetry-adapted eigenstates by an a posteriori process. The single_aniso module[41] of the MOLCAS package provides in fact the CF matrix in the $\{|J,m_J\rangle\}$ basis set, which produces the states and the energy levels obtained from the ab initio calculation. Using the threefold molecular axis as quantization axis, the $\langle J,m_J|\,\mathrm{CF}\,|J,m_J'\rangle$ elements that do not fulfil the condition $m_J' = m_J$, $m_J' = m_J \pm 3$, $m_J' = m_J \pm 6$, should be zero due to the symmetry. Therefore, we set to zero all those non-diagonal elements in the CF matrix, thereby giving rise to almost symmetry-adapted electronic states. By consequence, some degeneracy of the energy level structure is recovered, with some singlet states of the non-Kramers Ln^{3+} ions becoming doubly degenerate due to the increased symmetry.

Acknowledgements

The authors would like to thank the European Research Council for funding through the Advanced Grant MolNanoMaS (no. 267746), and the Italian MIUR for funding through the FIRB project (RBAP117RWN). M.-E.B. warmly acknowledges G. Cucinotta for assistance in fitting the single crystal magnetic measurements with the home-written program chirot2-2. J.L. thanks the Spanish MEC OM Project MAT11/27233-C02-02, and the resources from the supercomputer "Caesaraugusta", technical expertise and assistance provided by BIFI - Universidad de Zaragoza.

Keywords: crystal structures · density functional calculations · iron · lanthanides · magnetic anisotropy

[1] D. Gatteschi, R. Sessoli, J. Villain, *Molecular Nanomagnets*, Oxford University Press, New York, **2006**.

[2] a) S. Thiele, F. Balestro, R. Ballou, S. Klyatskaya, M. Ruben, W. Wernsdorfer, *Science* **2014**, *344*, 1135 – 1138; b) R. Vincent, S. Klyatskaya, M. Ruben, W. Wernsdorfer, F. Balestro, *Nature* **2012**, *488*, 357 – 360.

[3] a) J. M. Zadrozny, D. J. Xiao, M. A. Atanasov, G. J. Long, F. Grandjean, F. Neese, J. R. Long, *Nat. Chem.* **2013**, *5*, 577 – 581; b) C. J. Milios, A. Vinsla-

va, W. Wernsdorfer, S. Moggach, S. Parsons, S. P. Perlepes, G. Christou, E. K. Brechin, *J. Am. Chem. Soc.* **2007**, *129*, 2754 – 2755.

[4] a) D. N. Woodruff, R. E. P. Winpenny, R. A. Layfield, *Chem. Rev.* **2013**, *113*, 5110 – 5148; b) J. Luzon, R. Sessoli, *Dalton Trans.* **2012**, *41*, 13556 – 13567.

[5] a) C. R. Ganivet, B. Ballesteros, G. de La Torre, J. M. Clemente-Juan, E. Coronado, T. Torres, *Chem. Eur. J.* **2013**, *19*, 1457 – 1465; b) J. D. Rinehart, M. Fang, W. J. Evans, J. R. Long, *J. Am. Chem. Soc.* **2011**, *133*, 14236 – 14239; c) R. J. Blagg, C. A. Muryn, E. J. L. McInnes, F. Tuna, R. E. P. Winpenny, *Angew. Chem. Int. Ed.* **2011**, *50*, 6530 – 6533; *Angew. Chem.* **2011**, *123*, 6660 – 6663.

[6] J.-L. Liu, J.-Y. Wu, Y.-C. Chen, V. Mereacre, A. K. Powell, L. Ungur, L. F. Chibotaru, X.-M. Chen, M.-L. Tong, *Angew. Chem. Int. Ed.* **2014**, *53*, 12966 – 12970; *Angew. Chem.* **2014**, *126*, 13180 – 13184.

[7] J. D. Rinehart, J. R. Long, *Chem. Sci.* **2011**, *2*, 2078 – 2085.

[8] a) N. F. Chilton, D. Collison, E. J. L. McInnes, R. E. P. Winpenny, A. Soncini, *Nat. Commun.* **2013**, *4*, 2551; b) N. F. Chilton, R. P. Anderson, L. D. Turner, A. Soncini, K. S. Murray, *J. Comput. Chem.* **2013**, *34*, 1164 – 1175.

[9] N. F. Chilton, C. Goodwin, D. P. Mills, R. E. P. Winpenny, *Chem. Commun.* **2015**, *51*, 101 – 103.

[10] a) J. J. Baldoví, S. Cardona-Serra, J. M. Clemente-Juan, E. Coronado, A. Gaita-Aríño, A. Palii, *J. Comput. Chem.* **2013**, *34*, 1961 – 1967; b) J. J. Baldoví, J. M. Clemente-Juan, E. Coronado, Y. Duan, A. Gaita-Aríño, C. Giménez-Saiz, *Inorg. Chem.* **2014**, *53*, 9976 – 9980.

[11] a) M.-E. Boulon, G. Cucinotta, J. Luzon, C. Degl'Innocenti, M. Perfetti, K. Bernot, G. Calvez, A. Caneschi, R. Sessoli, *Angew. Chem. Int. Ed.* **2013**, *52*, 350 – 354; *Angew. Chem.* **2013**, *125*, 368 – 372; b) G. Cucinotta, M. Perfetti, J. Luzon, M. Etienne, P.-E. Car, A. Caneschi, G. Calvez, K. Bernot, R. Sessoli, *Angew. Chem. Int. Ed.* **2012**, *51*, 1606 – 1610; *Angew. Chem.* **2012**, *124*, 1638 – 1642.

[12] L. Rigamonti, M. Piccioli, L. Malavolti, L. Poggini, M. Mannini, F. Totti, B. Cortigiani, A. Magnani, R. Sessoli, A. Cornia, *Inorg. Chem.* **2013**, *52*, 5897 – 5905.

[13] A.-L. Barra, A. Caneschi, A. Cornia, F. Fabrizi de Biani, D. Gatteschi, C. Sangregorio, R. Sessoli, L. Sorace, *J. Am. Chem. Soc.* **1999**, *121*, 5302 – 5310.

[14] S. Accorsi, A.-L. Barra, A. Caneschi, G. Chastanet, A. Cornia, A. C. Fabretti, D. Gatteschi, C. Mortalo, E. Olivieri, F. Parenti, P. Rosa, R. Sessoli, L. Sorace, W. Wernsdorfer, L. Zobbi, *J. Am. Chem. Soc.* **2006**, *128*, 4742 – 4755.

[15] L. Sorace, M.-E. Boulon, P. Totaro, A. Cornia, J. F. Soares, R. Sessoli, *Phys. Rev. B* **2013**, *88*, 104407.

[16] P. Totaro, K. C. M. Westrup, M.-E. Boulon, G. G. Nunes, D. F. Back, A. Barison, S. Ciattini, M. Mannini, L. Sorace, J. F. Soares, A. Cornia, R. Sessoli, *Dalton Trans.* **2013**, *42*, 4416 – 4426.

[17] K. C. M. Westrup, M.-E. Boulon, P. Totaro, G. G. Nunes, D. F. Back, A. Barison, M. Jackson, C. Paulsen, D. Gatteschi, L. Sorace, A. Cornia, J. F. Soares, R. Sessoli, *Chem. Eur. J.* **2014**, *42*, 4416 – 4426.

[18] N. F. Chilton, S. K. Langley, B. Moubaraki, K. S. Murray, *Chem. Commun.* **2010**, *46*, 7787 – 7789.

[19] L. Rigamonti, A. Cornia, A. Nava, M.-E. Bolulon, M. Perfetti, A.-L. Barra, X. Zhong, K. Park, R. Sessoli, *Phys. Chem. Chem. Phys.* **2014**, *16*, 17220 – 17230.

[20] **Fe_3Yb** was obtained as crystals suitable for X-ray diffraction, but refinement was unsatisfactory because of major disorder effects. In particular, a large electron density residual (4 e Å^{-3}) was found at short distance (1 Å) from the Yb ion along the threefold axis. We thus suspect that this derivative is not isomorphous with the rest of the series and that the small radius forces the Yb ion to lie off-center in the cage defined by tea^{3-} ligands. This structure deserves further studies and we prefer to present the data in a separate publication.

[21] L. Gregoli, C. Danieli, A.-L. Barra, P. Neugebauer, G. Pellegrino, G. Poneti, R. Sessoli, A. Cornia, *Chem. Eur. J.* **2009**, *15*, 6456 – 6467.

[22] I. J. Hewitt, J. Tang, N. T. Madhu, C. E. Anson, Y. Lan, J. Luzon, M. Etienne, R. Sessoli, A. K. Powell, *Angew. Chem. Int. Ed.* **2010**, *49*, 6352 – 6356; *Angew. Chem.* **2010**, *122*, 6496 – 6500.

[23] F. Neese, The ORCA program system, *WIREs Comput. Mol. Sci.* **2011**, *2*, 73 – 78.

[24] a) B. O. Roos, P. R. Taylor, P.E.M. Siegbahn, *Chem. Phys.* **1980**, *48*, 157– 173; b)P.A. Malmqvist, B. O. Roos, B. Schimmelpfennig, *Chem. Phys. Lett.* **2002**, *357*, 230–240.

[25] G. Karlström, R. Lindh, P. A. Malmqvist, B. O. Roos, U. Ryde, V. Veryazov, P. O. Widmark, M. Cossi, B. Schimmelpfennig, P. Neogrady, L. Seijo, *Comput. Mater. Sci.* **2003**, *28*, 222 – 239.

[26] S. Vancoillie, P.-Å. Malmqvist, K. Pierloot, *ChemPhysChem* **2007**, *8*, 1803 – 1815.

[27] N. Ishikawa, M. Sugita, T. Ishikawa, S. Koshihara, Y. Kaizu, *J. Am. Chem. Soc.* **2003**, *125*, 8694 – 8695.

[28] a) M. A. AlDamen, J. M. Clemente-Juan, E. Coronado, C. Martí-Gastaldo, A. Gaita-Ariño, *J. Am. Chem. Soc.* **2008**, *130*, 8874–8875; b)J.M. Clemente-Juan, E. Coronado, A. Gaita-Ariño, *Chem. Soc. Rev.* **2012**, *41*, 7464–7478.

[29] a) S.-D. Jiang, B.-W. Wang, H.-L. Sun, Z.-M. Wang, S. Gao, *J. Am. Chem. Soc.* **2011**, *133*, 4730–4733; b)K.R. Meihaus, J. R. Long, *J. Am. Chem. Soc.* **2013**, *135*, 17952–17957.

[30] P. Zhang, L. Zhang, C. Wang, S. Xue, S.-Y. Lin, J. Tang, *J. Am. Chem. Soc.* **2014**, *136*, 4484 – 4487.

[31] a) J. R. Witt, E. I. Onstott, *J. Inorg. Nucl. Chem.* **1962**, *24*, 637 – 639; b) X.-L. Zhu, G. Wu, Z.-C. Qiu, Y. Zhou, J. Gong, K.-K. Yang, Y.-Z. Wang, *J. Polym. Sci. Part A* **2008**, *46*, 5214 – 5222.

[32] a) A. Altomare, G. Cascarano, C. Giacovazzo, A. Guagliardi, *J. Appl. Crystallogr.* **1993**, *26*, 343 – 350; b) A. Altomare, G. Cascarano, C. Giacovazzo, A. Guagliardi, M. C. Burla, G. Polidori, M. Camalli, *J. Appl. Crystallogr.* **1994**, *27*, 435 – 436.

[33] a) G. M. Sheldrick, *SHELX97*, *Programs for Crystal Structure Analysis*, University of Göttingen, Göttingen, **1997**; b)G.M. Sheldrick, *Acta Crystallogr. Sect. A: Found. Cryst. Sect. A* **2008**, *64*, 112–122.

[34] a) L. J. Farrugia, *J. Appl. Crystallogr.* **1999**, *32*, 837 – 838; b) L. J. Farrugia, *J. Appl. Crystallogr.* **2012**, *45*, 849 – 854.

[35] C. F. Macrae, I. J. Bruno, J.A. Chisholm, P.R. Edgington, P. McCabe, E. Pidcock, L. Rodriguez-Monge, R. Taylor, J. van de Streek, P. A. Wood, *J. Appl. Crystallogr.* **2008**, *41*, 466–470.

[36] *Diamond*, *Crystal and Molecular Structure Visualization* Crystal Impact, Dr.H. Putz and Dr.K. Brandenburg GbR, Kreuzherrenstr. 102, 53227 Bonn, Germany: http://www.crystalimpact.com/diamond.

[37] G. A. Bain, J. F. Berry, *J. Chem. Educ.* **2008**, *85*, 532 – 536.

[38] F. J. Neese, *Chem. Phys.* **2001**, *115*, 11080 – 11096.

[39] A. Schäfer, C. Huber, R. Ahlrichs, *J. Chem. Phys.* **1994**, *100*, 5829 – 5835.

[40] J. P. Perdew, *Phys. Rev. B* **1986**, *33*, 8822 – 8824.

[41] a) L. F. Chibotaru, L. Ungur, C. Aronica, H. Elmoll, G. Pilet, D. Luneau, *J. Am. Chem. Soc.* **2008**, *130*, 12445 – 12455; b) Program SINGLE ANISO, L. F. Chibotaru, L. Ungur, University of Leuven (Belgium) **2006**.